Physical Sensitivity of Silica Micro-Cantilevers Fabricated using Direct UV Writing and Micromachining

Christopher HOLMES, Lewis G. CARPENTER, Helen L. ROGERS, James C. GATES and Peter G. R. SMITH

Optoelectronics Research Centre, University of Southampton, SO17 1BJ, UK
E-mail: chh@orc.soton.ac.uk

A silica micro-cantilever with intrinsically defined planar Bragg gratings has been fabricated using a combination of direct UV writing and micromachining, in a silica-on-silicon platform. Through optically monitoring the response of the Bragg gratings, defined within the cantilever, induced stresses can be measured. The fabricated silica cantilever is 65 μm wide, 40 μm thick and 3 mm in length. It contains three planar Bragg gratings and can attain ~60 nm deflection resolution.

Keywords: Direct UV writing, planar Bragg gratings, micro-cantilever

1. Introduction

Micro-cantilevers are ubiquitous in physical, chemical and biological sensing. They have received increasing interest over recent years, as a new type of miniaturised transducer that is easy-to-use, cheap and highly sensitive.

Micro-cantilevers are used to measure physical, chemical and biological changes through their impact on the properties of the deflectable cantilever structure. The positional change of the structure may be measured by either electronic or optical means [1].

Deflection detection using electronic means include piezoresistive [2,3] and capacitive [4] techniques. These have the advantage of being able to integrate the device on a single compact chip. However, the deflection resolution is typically less than optical methods. In addition, optical devices possess the ability to function in flammable environments without the risk of ignition and have immunity to electromagnetic interference.

Optical detection is typically achieved through free-space optical levering [5], inteferometry [6,7] or the use of diffraction gratings [8]. These methods of detection are typically 'free-space' as the optical wave is not guided by the cantilever structure, which usually means the device can not be integrated upon a single compact chip. The work reported in this paper considers a planar silica micro-cantilever that guides light within the cantilevers physical structure. The reported device is fabricated from a silica-on-silicon chip, which has the inherent advantage of integration.

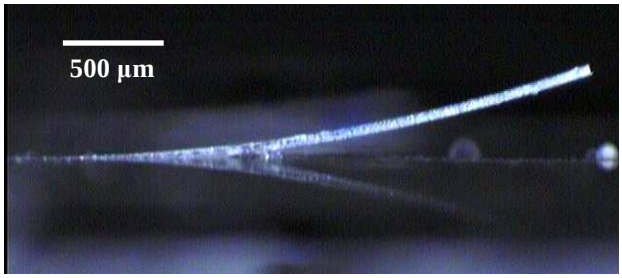

Fig. 1 Optical microscope image of the silica cantilever

The fabricated silica micro-cantilever, pictured in Figure 1, has of a direct UV written optical waveguide and a series of Bragg gratings defined intrinsically within it. Applying stress to the cantilever results in a physical change in the Bragg gratings. Through monitoring the reflection spectra of the Bragg gratings the applied stress in the cantilever can be measured and thus its deflection obtained.

2. Design and Fabrication

Device fabrication is uniquely achieved through a combination of direct UV writing and micromachining in a silica-on-silicon platform. The combination of these novel techniques allow for rapid prototyping, as they do not require photolithography steps that can be expensive and time consuming, particularly for small device quantities.

Direct UV Writing (DUW) has been used to simultaneously fabricate waveguides and Bragg gratings. The first stage of conventional DUW is the deposition of two silica layers upon a silicon wafer, which is ~1 mm thick and has a thick (17 μm) thermally grown oxide. The silica layers are deposited using a flame hydrolysis deposition (FHD) technique and subsequently consolidated at ~1300°C. The first deposited silica layer was 7 μm thick and doped with germanium, the second silica layer was 17 μm thick and had no germanium doping. The composition of the substrate is illustrated in Figure 2.

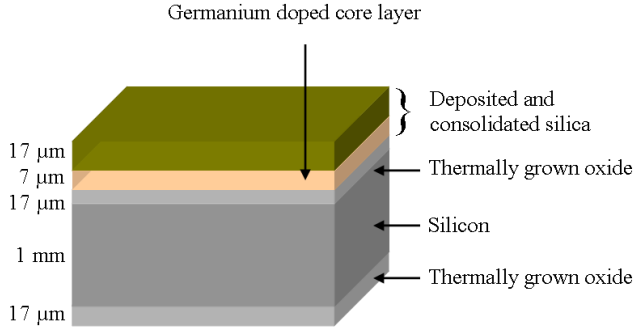

Fig. 2 Composition of the silica-on-silicon substrate

The first deposited layer (core layer) is effectively sandwiched between two layers of silica, the thermally grown silica and the final FHD layer. This core silica layer is the only one of the three layers doped with germanium and is consequently photosensitive to UV radiation. The layer is 7 μm thick to ensure vertical single mode confinement, at C-band wavelengths. In addition other dopants (boron and phosphorus) are used to control refractive index of the core and overclad layers.

It must be noted that the thick thermal oxide acts to aid the adhesion of the deposited silica. Its thickness also acts as a low refractive index buffer layer (underclad) for light-waves guiding in the core layer.

The next stage of fabrication is the definition of waveguides and planar Bragg grating elements using DUW. The DUW method, used in the fabrication of the following devices, is a dual beam Direct Grating Writing (DGW) variant of DUW [9]. The established technique is ideally suited to rapid prototyping, requiring no photolithograph or etching and as a result no specialized cleanroom facilities.

DGW can define both waveguide and planar Bragg grating structures in a single step process. The technique focuses two coherent laser beams to a ~7 μm diameter spot within the germanium-doped silica layer. As the beams are coherent an interference pattern is achieved at the focused spot. By traversing the sample beneath the spot, waveguides can be directly written into the photosensitive germanium-doped silica core layer. More interestingly, by amplitude modulating the exposure during translation planar Bragg grating structures can be written, as illustrated in Figure 3. As DGW is computer controlled, the time required from initial circuit concept to completed fabrication takes in the order of minutes and not days as is true for alternative photolithograph methods.

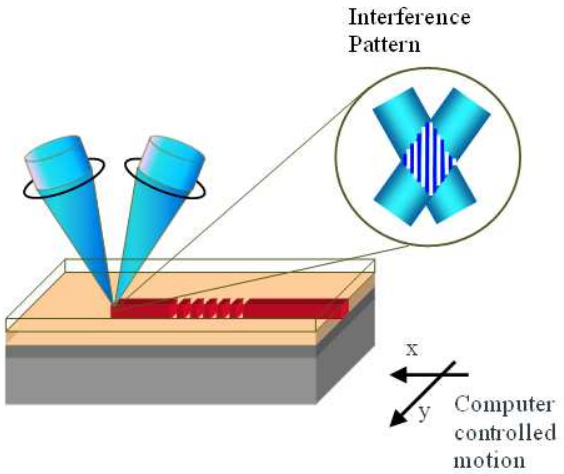

Fig. 3 Composition of silica-on-silicon wafer

In the fabrication of these silica micro-cantilevers, we choose to create physical grooves in the substrate before the DGW process. The grooves were fabricated using a precision dicing saw and created the cantilever's outline into the substrate, illustrated in Figure 4 (a). The cuts were made using a 30 μm wide metal bonded diamond dicing blade with an outer diameter of 54 mm. The grooves were 60 μm deep, such to expose the underlying silicon. Once the grooves were created UV writing was used to add the channels and Bragg gratings.

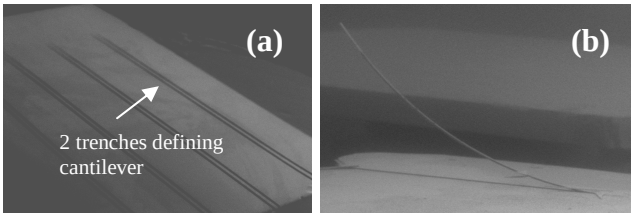

Fig. 4 Scanning Electron Microscope images of (a) diced grooves defining the outline of four cantilevers and (b) a cantilever released from the underlying silicon after etching

In the final stage of fabrication a silicon etchant (KOH) was used to liberate the silica cantilever from the underlying silicon, as illustrated in Figure 4 (b). This etch process took 9 hours at 70°C, with 1.0 M of KOH solution. The resulting cantilever was 65 μm wide and 40 μm thick. The cross-sectional dimensions ensured that the evanescent field of the waveguide mode was not exposed to the surrounding medium. Thus, the spectral response of the Bragg gratings within the cantilever were only affected by induced stresses, either internal (i.e. thermal expansion) or external (i.e. applied load).

The cantilever chip reported in this paper consisted of seven single mode planar Bragg gratings, each 1 mm in length and placed end-to-end. Three of the Bragg gratings were located on the cantilever and four on the main body of the cantilever, as illustrated in Figure 5.

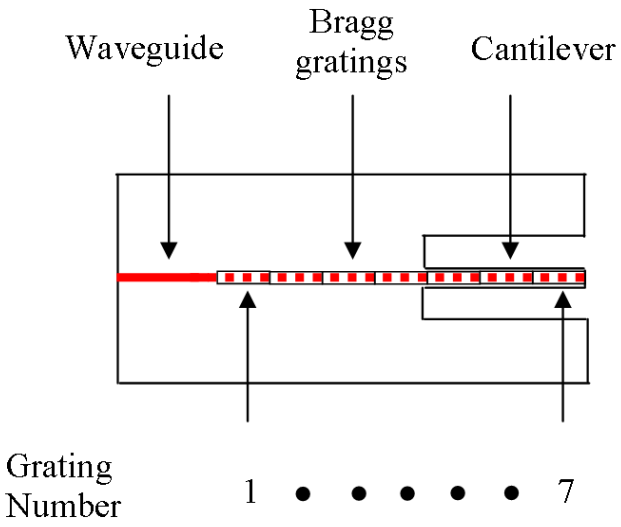

Fig. 5 Top view of cantilever chip design, showing locations of seven Bragg gratings with respect to cantilever body

The seven Bragg gratings were all Gaussian apodised and written such that they were sequentially separated spectrally by 5 nm. The Bragg grating with the lowest central wavelength was the one physically furthest from the cantilever, i.e. grating number 1 in Figure 5.

It must be noted that this proof of principle silica cantilever has a 3 mm length. However, using this technique sub-millimetre length cantilevers can also be realised.

To launch light into the device, a silicon V-groove containing a prealigned single-mode fiber was aligned to the waveguide and secured using a UV epoxy. The fiber V-groove assembly was aligned to give optimum coupling and after attachment was mechanically robust.

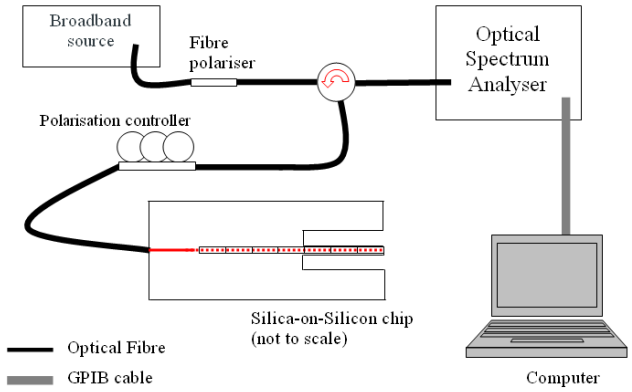

Fig. 6 Optical Interrogation system

The optical spectra of the Bragg gratings was monitored in reflection using a broadband source, optical circulator and optical spectrum analyzer (OSA), as illustrated in Figure 6.

Using a polarizer and polarization controller Transverse Electric (TE) and Transverse Magnetic (TM) polarizations can be monitored independently. The data captured by the optical spectrum analyzer was sent via a GPIB cable to a computer which interrogated the data using Labview software.

The spectral resolution of the OSA was set to 1 pm resolution. Through fitting a Gaussian curve to the collected data and temperature referencing, the uncertainty of the central Bragg wavelengths can be reduced to 0.1 pm.

The TE reflection spectrum of the direct UV written planar Bragg gratings, before and after the KOH etching stage, is illustrated in Figure 7. The four peaks with lower central wavelengths are from gratings located on the main body of the chip. The three peaks with higher wavelengths are from gratings on the cantilever. It can be observed that whilst the gratings on the main body of the chip have shifted little, all the gratings on the cantilever have shifted to higher wavelengths after the etching stage.

The large spectral shifts occurring after etching for the gratings on the cantilever are understood to result from the removal of the thermal stress mismatch at the silica-silicon interface, during the silicon etching stage.

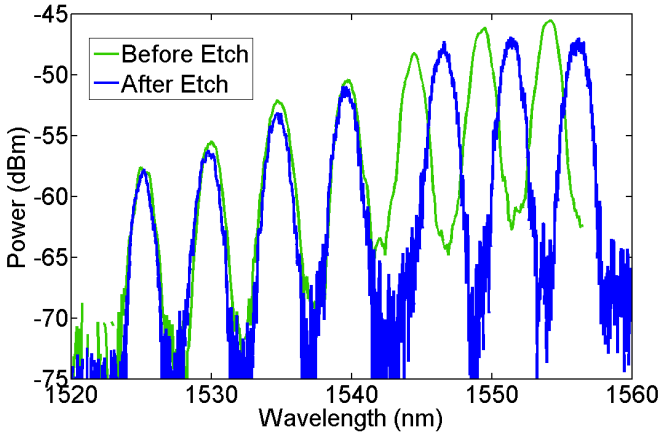

Fig. 7 Optical reflection spectrum of TE mode

3. Thermal Stress Missmatch

Thermal stress mismatch is understood to occur in FHD samples as a result of the high consolidation temperatures (~1300°C) and the difference in expansion coefficient between silica (4.9×10^{-7} °C^{-1}) and silicon (2.6×10^{-6} °C^{-1}) [10]. This can be expressed in terms of strain as

$$\varepsilon = (\alpha_{SiO2} - \alpha_{Si})\Delta T \qquad (1)$$

where ε is the uni-directional strain along the silica-silicon interface, α is the thermal expansion coefficients (subscripts indicating for silica SiO_2 and silicon Si respectively), ΔT is the temperature difference between consolidation and operation temperature. From Equation 1 it can be calculated that the thermal strain mismatch is 2500 με, which corresponds to a thermal stress mismatch in the silica of 180 MPa.

The thermal stress mismatch, which is relieved after etching, can be theoretically treated to infer the expected spectral change. The spectral change of a direct UV written Bragg grating to applied strain is understood to respond in a spectral shift Δλ defined by [11]

$$\frac{\Delta\lambda_{x,y}}{\lambda_{x,y}} = \varepsilon_z - \frac{n_{x,y}^{\ 2}}{2}\left(p_{11}\varepsilon_{x,y} + p_{12}(\varepsilon_z + \varepsilon_{y,x})\right) \qquad (2)$$

where subscripts x and y are the transverse and longitudinal directions for a wave propagating along z, p_{11} and p_{12} are elements of the stress optic tensor, in this instance taken for silica. It must be noted that λ_x and λ_y represent the TE and TM polarizations respectively and thus n_x and n_y are the effective indices for TE and TM modes respectively. Calculating the induced strains from the thermal stress mismatch and placing them into Equation 2 results theoretically in a TE wavelength shift of 2.67 nm. Figure 8 shows the measured central Bragg wavelengths (taken from data shown Figure 7) for the seven planar Bragg gratings before and after etching. The average wavelength shift for the cantilever gratings is 2.68 nm, which agrees well with the theoretical prediction of 2.67 nm.

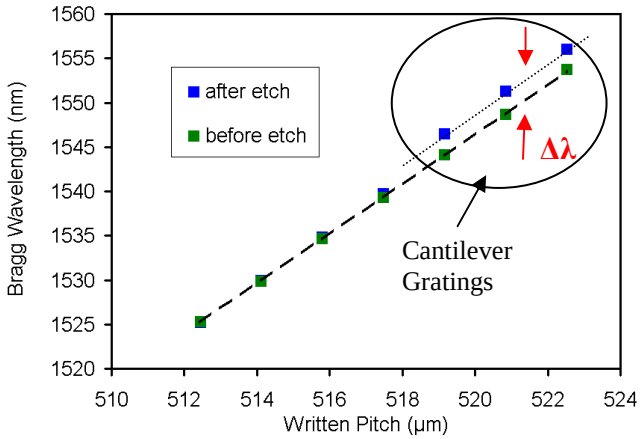

Fig. 8 Central Bragg wavelength of the seven gratings before and after etching

Rearranging Equation 2 and assuming that $n_x \approx n_y$, the theoretical spectral change in birefringence is

$$\Delta(n_x - n_y) = \frac{n^3}{2}\left[(p_{11} - p_{12})(\varepsilon_x - \varepsilon_y)\right] \qquad (3)$$

where n is the average effective index for the TE and TM mode.

The calculated theoretical birefringence shift resulting from the relief of thermal stress mismatch is -3.30 x 10^{-4}. As seen in Figure 9, which shows the birefringence after etching for the seven gratings, this agrees with measured data. Grating numbers 1-4 are on the chip so have not had thermal stress mismatch relieved, whilst grating 5-7 are on the cantilever and show a birefringence shift of -3.35 x 10^{-4}.

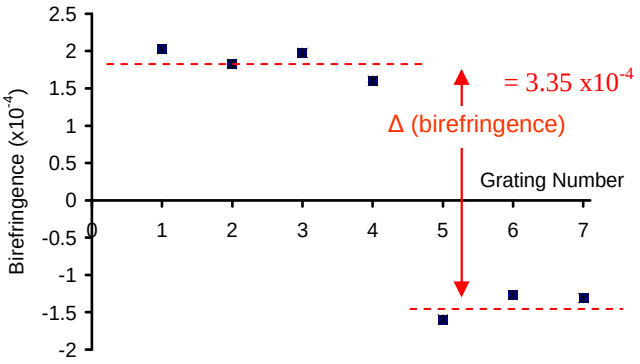

Fig. 9 Optical Interrogation system

So far stress monitoring has looked at the release of thermal stress mismatch as a result of fabrication. The following section shall consider stress induce deflections from externally applied load.

4. Point Load

The following section considers the application of a point load on the cantilever, as illustrated schematically in Figure 10. Load was applied to the actual cantilever using a KLA Tencor P16 stylus profiler. This can apply loads to the cantilever and map the respective deflection. Thus the profiler allows two important physical parameters of the cantilever to be quantified, the spring constant and the deflection sensitivity.

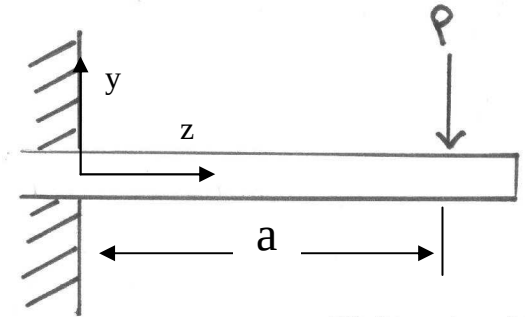

Fig. 10 Method of applied load P

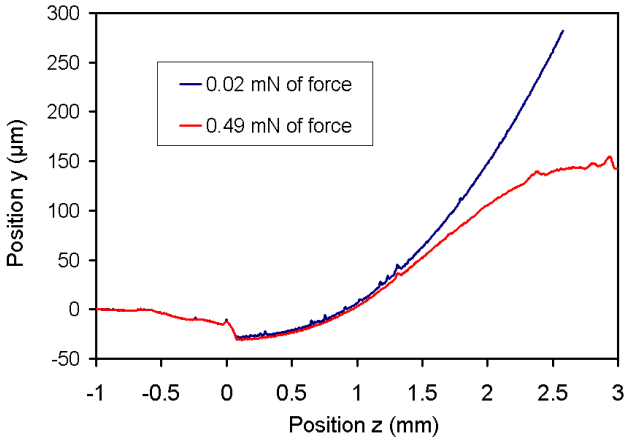

Fig. 11 Positional information of stylus profiler

The deflection in the vertical position *y* for two different applied forces along the horizontal position *z* is given in Figure 11. It must be noted that the stylus profiler has scanned 1 mm of bulk chip before scanning the cantilever. Hence the cantilever begins at position z equal to 0 mm. In addition the data is restricted by the profiler's vertical range of 300 µm and hence scan of 20 µN applied load does not sweep the total length of the cantilever as the initial static deflection is greater than the range. As can be seen from Figure 1 this static deflection, which was due to thermal stress mismatch, was 410 µm. For the scan of 490 µN applied load the deflection was greater and was not restricted by the profiler's vertical range.

The spring constant *k* is a fundamental property of the cantilever. It yields the stiffness of the cantilever and is the proportionality factor between applied force, *P* and the resulting bending of the cantilever, Δ*y*. This relation is called Hooke's law.

$$P = -k\Delta y \qquad (4)$$

For an applied force of 490 µN at the end of the cantilever the resulting deflection is 260 µm. From Equation 4 this relates to a spring constant of 1.9 Nm^{-1}. The theoretical spring constant for a rectangular cantilever of length L, can be calculated as

$$k = \frac{3EI}{L^3} \qquad (5)$$

where *E* is the Young's modulus and *I* is the moment of cross-sectional area. The theoretical spring constant for the silica micro-cantilever is 2.7 Nm^{-1}, which is comparable to the measured value. For this calculation it is assumed that the cantilever is straight, not one with static deflection, which for this case results from thermal stress mismatch.

By collating the reflection spectra during different applied positional loads the optical deflection resolution can be obtained. Figure 12 shows the spectral shifts of Bragg grating numbers 1 and 6 for TE polarization, as a result of a 490 µN load being applied at horizontal position *z*. It must be noted that grating numbers 2 – 4 (gratings on the main

chip) all had negligible response, just as is observed with grating number 1.

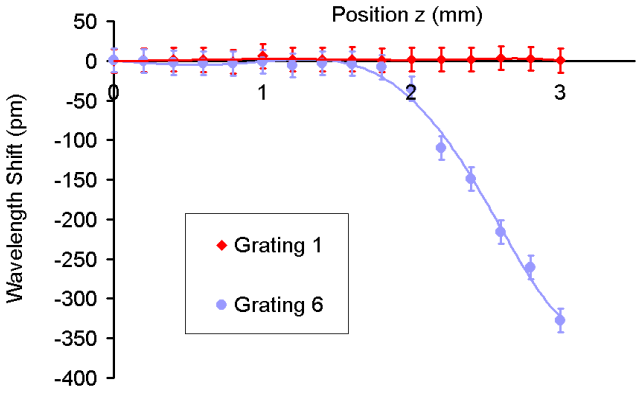

Fig. 12 Optical response of stylus profiler

The moment *M* that occurs at position *z* on the cantilever, resulting from an applied load *P* at position *a*, can be defined as

$$M(z) = \begin{cases} Pa\left(1 - \dfrac{z}{a}\right) & 0 \le z \le a \\ 0 & a < z \le L \end{cases} \qquad (6)$$

It is understood that induced strain is directly proportional to the moment [11]. Thus, from Equations 2 and 6 the spectral response of gratings 5 - 7 is expected to be asymmetric. The grating at location *z* on the cantilever is expected to show no spectral response when $a \le z$ and a linearly proportional response that is negative in magnitude for $a > z$. As can be seen in Figure 12 the measured response agrees with this theory.

For the condition *z* > *a* the spectral shift per fractional change in distance is expected to be equal for all gratings. Thus grating 5 is expected to show the greatest total spectral shift. However, due to the curvature of the dicing blade, the cantilever structure around grating 5 detaches in a tapered fashion, i.e. the cantilever outline is only fully detached from the chip at z ~ 0.4 mm. This means the strain per fractional change in load position is less for grating 5 than it is for 6 and 7. Indeed, the spectral shift per fractional change in load for grating 5 was measured to be -0.3×10^{-6} compared to -2.7×10^{-6} and -2.8×10^{-6} for gratings 6 and 7 respectively. Thus, grating number 6 has the greatest displacement sensitivity.

The maximum spectral shift for grating number 6 is 410 pm for TM polarization. This occurs at a maximum end point deflection of 260 μm. Meaning the total deflection detection of this silica cantilever, considering the resolution achievable with thermally compensated Bragg gratings, is ~60 nm.

5. Conclusions

An effective silica cantilever with inherently defined planar Bragg gratings has been fabricated.

The Bragg gratings have been used to quantify thermal stress mismatch, the experimental result agrees with that theoretically expected.

From deflection data the spring constant of the cantilever has been obtained as 1.9 Nm^{-1}, which is comparable to the theoretical spring constant of the structure.

The deflection sensitivity of the device is ~60 nm. Further enhancement of Bragg gratings with respect to the neutral axis of the cantilever may further enhance this sensitivity.

It has been seen that using a series of multiplexed gratings the variation of stress along the cantilever can be quantified. This can be used to locate a point load on the cantilever or a more complicated distributed load pattern.

Acknowledgments and Appendixes

The author's thank the Engineering and Physical Science Research Council (EPSRC) for their financial support on this project.

References

[1] N.V. Lavrik, M.J. Sepaniak, P.G. Datskos, Review of Scientific Instruments, 75, (2004), 7.
[2] J. Thaysen, A. Boisen, O. Hansen and S. Bouwstra, Sens. Actuators A, 83, (2000).
[3] M. Yang, X. Zhang, K. Vafai, and C.S. Ozkan, J. Micromech. Microeng., 13, (2003).
[4] N. Blanc, J.Brugger, N.F.D. Rooij and U. Durig, J Vac. Sci. Technol. B, 14, (1996), 2.
[5] G. Meyer and N.M. Amer, Appl. Phys. Lett., 53, (1988), 12.
[6] R. Erlandsson, G.M. McClelland, C.M. Mate, and S. Chiang, J. Vac. Sci. Technol. A, 6, (1988), 2.
[7] D. Rugar, H.J. Mamin and P. Guethner, Appl. Phys. Lett., 55, (1989), 25.
[8] S.R. Manalis, S.C. Minne, A. Atalar and C.F. Quate, Appl. Phys. Lett, 69, (1996), 25.
[9] G.D. Emmerson, S. P. Watts, C. B.E. Gawith, V. Albanis, M. Ibsen, R. B. Williams and P. G.R. Smith, Elec. Lett, 38, (2002) 24.
[10] L. Eckertova, "Physics of thin films", second ed. (Plenum, 1995).
[11] C. Holmes, J.C. Gates, C.B.E. Gawith, P.G.R. Smith, Opt. Eng., 49 (4), 2009,